Engineering Fracture Mechanics 89 (2012) 24–39

Contents lists available at SciVerse ScienceDirect

Engineering Fracture Mechanics

journal homepage: www.elsevier.com/locate/engfracmech

Further results in *J* and CTOD estimation procedures for SE(T) fracture specimens – Part II: Weld centerline cracks

Marcelo Paredes, Claudio Ruggieri *

Department of Naval Architecture and Ocean Engineering, Av. Prof. Mello Moraes, 2231 (PNV-EPUSP), São Paulo 05508-030, Brazil

ARTICLE INFO

Article history:
Received 15 July 2011
Received in revised form 23 December 2011
Accepted 29 March 2012

Keywords:
J-integral
CTOD
Eta-factor
SE(T) specimen
Weld strength mismatch

ABSTRACT

This work examines the effect of weld strength mismatch on *J* and CTOD fracture parameters using single edge notch tension (SE(T)) specimens. A central objective of the study is to enlarge on previous *J* and CTOD estimation procedures based upon plastic *eta* factors (η) described in Part I for centerline-cracked welds. The present analyses provide a large set of η-factors for a wide range of crack sizes (a/W-ratio) and material properties, including different levels of weld strength mismatch, which are applicable in improved estimation equations for *J* and CTOD for weld centerline notched SE(T) specimens.

1. Introduction

Structural integrity assessments of steel weldments (weld metal and heat affected zone – HAZ) remain a key issue for the safety analyses of critical welded structures, including pressure vessels, piping systems and storage tanks. Experimental observations consistently reveal the occurrence of crack-like defects in the welded region which are either planar (e.g., hot or cold cracking, lack of penetration, undercut) or volumetric (e.g., porosity and entrapped slag). To address the potential deleterious effects of such defects on the structural integrity, many codes and current fabrication practices require the use of weldments with weld metal strength higher than the base metal strength; a condition referred to as overmatching. An evident benefit and primary motivation to use weld overmatching is to promote gross section yielding of the base plate due to the higher yield stress of the weld metal. This has the effect of limiting the higher stresses that would otherwise occur in a homogeneous material thereby shielding the welded region. Moreover, the overmatch weld also causes the large plastic deformation field to shift into the lower strength base metal where the fracture resistance is presumably higher and fewer defects occur.

Fracture mechanics based approaches to describe ductile fracture behavior in structural components, including welded structures, rely upon crack growth resistance (J-Δa) curves (also termed *R*-curves) to characterize crack extension followed by crack instability of the material [1,2]. These approaches allow the specification of critical crack sizes based on the predicted growth of crack-like defects under service conditions. Current standardization efforts now underway [3–6] advocate the use of single edge notch tension specimens (often termed SE(T) or SENT crack configurations) to measure experimental *R*-curves more applicable to high pressure piping systems, including girth welds of marine steel risers. The primary motivation to use SE(T) fracture specimens in defect assessment procedures for this category of structural components is the strong similarity in crack-tip stress and strain fields which drive the fracture process for both crack configurations [7–11]. Recent

* Corresponding author.
E-mail address: claudio.ruggieri@usp.br (C. Ruggieri).

0013-7944/$ - see front matter © 2012 Elsevier Ltd. All rights reserved.
http://dx.doi.org/10.1016/j.engfracmech.2012.03.010

Nomenclature

a	crack depth
b	remaining crack ligament
m	dimensionless constant which relates J and CTOD
m_{SSY}	dimensionless constant which relates J and CTOD under small scale yielding
n	Ramberg–Osgood strain hardening exponent
A_p	plastic area under the load displacement curve
B, B_N	specimen thickness, effective thickness
$\overline{B}$	strain–displacement matrix based on the B-bar formulation
BM	base metal
CMOD	crack mouth opening displacement
CTOD	crack tip opening displacement
C(T)	compact tension specimen
C_k	coefficients for the polynomial fitting of factor η
E, E'	Young's modulus under plane stress (plane strain) conditions
G	crack geometry function
D	material deformation function
H	specimen length (distance between pins or clamps)
J	J-integral
J_2	second invariant of the stress deviator tensor
J_c	critical value of J-integral
J_D	value of J-integral based on a domain procedure
J_e	elastic component of J-integral
J_M	value of J-integral based on a multispecimen procedure
J_p	plastic component of J-integral
K_I	stress intensity factor
LLD	load-line displacement
M_y	weld strength mismatch ratio
P	applied load
SE(B)	single edge notch bend specimen
SE(T)	single edge notch tension specimen
U_p	potential energy for the cracked body
V	crack mouth opening displacement
V_e	elastic component of crack mouth opening displacement
V_p	plastic component of crack mouth opening displacement
W	structural component width
WM	weld metal
δ	crack tip opening displacement
δ_c	critical value of crack tip opening displacement
δ_e	elastic component of crack tip opening displacement
δ_p	plastic component of crack tip opening displacement
Δ	load-line displacement
Δ_e	elastic component of load-line displacement
Δ_p	plastic component of load-line displacement
$\bar{\varepsilon}$	true (logarithmic) strain
ζ_k	coefficients for the polynomial fitting of factor C_k
η	nondimensional parameter describing the plastic contribution to the strain energy
ν	Poisson's ratio
ρ_0	initial crack tip blunting radius
$\bar{\sigma}$	true stress
σ_{ys}	yield stress

applications of SE(T) fracture specimens to characterize crack growth resistance properties in pipeline steels [12] have been effective in providing larger flaw tolerances and, at the same time, reducing the otherwise excessive conservatism which arises when measuring the material's fracture toughness based on high constraint, single edge notch bend (SE(B)) or compact tension (C(T)) specimens.

However, these previous test protocols employ J estimation expressions which are mainly applicable to SE(T) fracture specimens made of homogeneous materials. Only little effort has been expended in the past years (see, for example, the representative work of Kim and Budden [13]) to extend J estimation procedures to testing of welded SE(T) specimens. For

a given specimen geometry, mismatch between weld metal and base plate strength affects the macroscopic mechanical behavior of the specimen in terms of its load–displacement response with a potentially strong impact on the coupling relationship between J (and, equivalently, the crack tip opening displacement, CTOD) and the near-tip stress fields. Moreover, the complex interaction between the local crack-tip fields (most often controlled by the flow properties of the weld metal) and the global plastic regime gives rise to near-tip constraint states which can differ significantly than the corresponding levels in crack-tip constraint for a homogeneous fracture specimen at the same (macroscopic) loading. In view of the technological importance of assessing fracture behavior in welded cracked structures using SE(T) fracture specimens, accurate estimation formulas for J and CTOD toughness parameters which are applicable to this crack configuration remain essential for more refined defect assessment procedures capable of including effects of weld strength mismatch on crack tip driving forces.

In Part I of this article [14], a large set of plastic η-factors applicable to evaluate J and CTOD in pin-loaded and clamped SE(T) specimens with varying a/W-ratios and hardening properties was developed. These dimensionless η-values enter directly into estimation procedures for fracture toughness based on experimentally measured plastic work as represented by the plastic area under the load–displacement curve derived from current testing protocols. Here, the plastic component of J, denoted J_p, is described in the form $J_p = \eta_J A_p/(B_N b)$, where A_p is the plastic area under the load vs. load-line displacement, B_N is the net specimen thickness, b is the uncracked ligament ($b = W - a$ where W is the thickness for the cracked configuration and a is the crack length). Factor η_J introduced by Sumpter and Turner [15] represents a nondimensional parameter which relates the plastic contribution to the strain energy for the cracked body with J and is assumed to be a function of the flawed configuration and independent of loading [16]. The approach is equally applicable when CTOD is used as the fracture parameter.

This work examines the effect of weld strength mismatch on fracture toughness measurements defined by J and CTOD fracture parameters using single edge notch tension (SE(T)) specimens. A central objective of the present study is to enlarge on previous developments of J and CTOD estimation procedures based upon plastic *eta* factors (η) already described in Part I for centerline-cracked welds. The present analyses enable the introduction of a large set of plastic η-factors for a wide range of crack sizes (as measured by the a/W-ratio) and material properties, including different levels of weld strength mismatch, characteristic of structural, pipeline and pressure vessel steels. Very detailed non-linear finite element analyses for plane-strain and 3-D models provide the evolution of load with increased load-line displacement to define the relationship between plastic work and crack-tip driving force (J and CTOD) for different weld mismatch levels from which the η-values are derived. Overall, the present results provide improved estimation equations for J and CTOD for weld centerline notched SE(T) specimens as a function of loading condition (pin load vs. clamped ends), crack geometry and strength mismatch levels.

2. *J* and CTOD estimation procedure

This section provides a brief overview and salient features of the adopted methodology to determine J and CTOD for SE(T) fracture with centerline-cracked, square grooved welds. Readers are referred to Part I of this article [14] for additional details. The description begins with the J-integral and CTOD analysis for a cracked body based upon the plastic work measured from load–displacement records, LLD (Δ) and CMOD (V). Subsequent development focuses on a J-integral evaluation procedure using a multispecimen scheme which is compared with J-values based on domain integral approaches.

2.1. Evaluation procedure for J and CTOD based on plastic work

The procedure to evaluate the J-integral from laboratory measurements of load–displacement records begins by considering the elastic and plastic contributions to the strain energy for a cracked body under Mode I deformation in the form

$$J = J_e + J_p \tag{1}$$

where the elastic component, J_e, is given by the usual relationship $J_e = K_I^2/E'$. Here, K_I denotes the (Mode I) elastic stress intensity factor for the cracked configuration and $E' = E/(1 - \nu^2)$ where E and ν are the (longitudinal) elastic modulus and Poisson's ratio. For an SE(T) specimen, Cravero and Ruggieri [4] provide analytical expressions for parameter K_I, dependent upon specimen geometry, crack size and loading condition (pin-loaded vs. clamped ends).

The plastic component, J_p, is derived from the plastic contribution to the strain energy (due to the crack) and J expressed as [15]

$$J_p = \frac{\eta_J A_p}{B_N b} \tag{2}$$

where A_p is the plastic area under the load vs. load-line displacement (which represents the plastic work, U_p) and b is the uncracked ligament ($b = W - a$ where a is the crack length). Factor η_J introduced by Sumpter and Turner [15] represents a nondimensional parameter which relates the plastic contribution to the strain energy for the cracked body with J and is assumed to be a function of the flawed configuration and independent of loading [2]. Fig. 1 illustrates the essential features of the estimation procedure for J_p for a weld centerline notched specimen. Here, we also note that A_p (and consequently η_J) can be defined in terms of LLD (Δ) data or CMOD (V) data. For definiteness, these quantities are denoted η_J^{LLD} and η_J^{CMOD}.

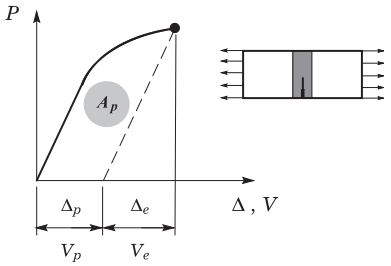

Fig. 1. Definition of the plastic area under the load–displacement (LLD or CMOD) curve for center notch welded specimens.

The previous framework also applies when the CTOD is adopted to characterize the crack-tip driving force by using the connection between J and the crack-tip opening displacement (δ) [17,18] given by

$$\delta = \frac{J}{m\sigma_{ys}} \tag{3}$$

in which m is a dimensionless constant. Consequently, a formally similar expression to Eq. (1) is employed to yield

$$\delta = \delta_e + \delta_p \tag{4}$$

where the elastic component, δ_e, is given by

$$\delta_e = \frac{K_I^2}{m_{ssy}\sigma_{ys}E'} \tag{5}$$

and the plastic component, δ_p, is expressed as

$$\delta_p = \frac{\eta_\delta^{\mathrm{CMOD}} A_p^{\mathrm{CMOD}}}{Bb\sigma_{ys}} \tag{6}$$

where factor $\eta_\delta^{\mathrm{CMOD}}$ represents a nondimensional parameter which describes the effect of plastic strain energy on the applied CTOD. In the above expressions, m_{SSY} is a plastic constraint factor relating J and CTOD under small scale yielding [2], σ_{ys} denotes the material's yield stress and parameter m represents a proportionality coefficient often used to relate the total value of J to the total value of CTOD which strongly depends on the material's strain hardening [17,24]. When the plastic component, δ_p, is evaluated based on the plastic hinge model such as in BS 7448 standard [19], factor m_{SSY} is most often assigned a value of 2.

The previous development based upon the η-factor concept retains strong contact with current standards to determine experimental J-values using common fracture specimens for homogeneous materials. Computation of η-factors for fracture specimens made of heterogeneous materials, such as the welded crack configuration displayed in Fig. 1, is relatively straightforward and depends upon the mismatch ratio, M_y, defined by

$$M_y = \frac{\sigma_{ys}^{WM}}{\sigma_{ys}^{BM}} \tag{7}$$

where σ_{ys}^{BM} and σ_{ys}^{WM} denote the yield stress for the base plate metal and weld metal.

2.2. Multispecimen measurements of plastic work

One of the first formal procedures to evaluate the J-integral using experimental measurements of load–displacement records was presented by Begley and Landes [20] using a multispecimens method to determine the variation in potential energy for a cracked body due to virtual crack extension. Here, the evaluation procedure for J is simply based on its energy interpretation in the form

$$J = -\frac{1}{B}\frac{dU_p}{da} \tag{8}$$

where U_p is the potential energy for the cracked body, B denotes the specimen thickness and a is the crack size. By considering fracture specimens with identical geometry and configuration (W and B) but with different initial crack lengths, the area under the load–displacement curve for each specified displacement increment, Δ_i, enables the construction of the relationship between the potential energy and crack size. Using the energy release rate definition expressed by previous Eq. (8), the J-integral with increased values of Δ for a given crack size, a, is simply evaluated from the derivative of Up with respect to the crack size. Part I of this article [14] illustrates the procedure to determine the J-integral based on the multispecimens methodology.

Although the method was originally adopted by Begley and Landes [20] as a natural procedure to determine J from experimentally measured load–displacement records using an extensive series of test specimens, it can also provide valuable insights when used in a numerical framework for both homogeneous and welded specimens. As will be addressed later in Section 5, this approach will be used to evaluate J from load–displacement records in the numerical models which is then compared to the line integral definition of J for a given crack configuration and strength mismatch level.

3. Numerical procedures

3.1. Plane-strain models of weld centerline cracked SE(T) specimens

Detailed finite element analyses are performed on plane-strain models for a wide range of conventional 1-T SE(T) fracture specimens (thickness $B = 25.4$ mm and $W = 2B = 50.8$ mm) under pin-loaded and clamped end conditions having a square groove weld with different groove width and weld strength mismatch. Fig. 2 shows the geometry and specimen dimensions for the analyzed crack configurations with different loading conditions, pin-loaded ends vs. clamped ends; these specimens are denoted as $SE(T)_P$ and $SE(T)_C$. Here, a is the crack size, W is the specimen width, H is the distance between the pin loading or clamps, $b = (W - a)$ represents the remaining crack ligament and $2h$ denotes the weld groove width. The analysis matrix includes SE(T) specimens having $a/W = 0.1$–0.7 with increments of 0.1, $H/W = 6$ (pin-loaded end), $H/W = 10$ (clamped ends) and weld groove width, $2h = 15$ mm. To assess the effect of weld groove size on the crack-tip driving forces, the analyses also consider groove width values in the range $10\text{ mm} \leqslant 2h \leqslant 40$ mm (i.e., $h/W = 0.1$, 0.15, 0.20 and 0.40 since W is fixed in the present analyses).

Fig. 3 shows the finite element models constructed for the plane-strain analyses of the deeply-cracked SE(T) specimens for pin-load and clamp conditions with $a/W = 0.5$ and a centerline-cracked, square-grooved weld with $2h = 15$ mm. The weld fracture specimen is modeled as a bimaterial component with no transition region, i.e., the mechanical properties for the heat affected zone (HAZ) are not considered. All other crack models have very similar features. A conventional mesh configuration having a focused ring of elements surrounding the crack front is used with a small key-hole at the crack tip; the radius of the key-hole, ρ_0, is 2.5 μm (0.0025 mm). Symmetry conditions permit modeling of only one-half of the weld centerline notched specimens with appropriate constraints imposed on the remaining crack ligament. A typical half-symmetric model has one thickness layer of ~3000 8-node, 3-D elements (~6400 nodes) with plane-strain constraints imposed ($w = 0$) on each node.

These finite element models are loaded by displacement increments imposed on the loading points to enhance numerical convergence and to provide a closer correspondence with the actual experimental conditions at the specimen ends. Further, the numerical analyses for the pin-loaded specimens also incorporate the contact interaction between the loading pin (represented as a rigid cylinder) and the specimen (see Fig. 3).

3.2. 3-D models of weld centerline cracked SE(T) specimens

Finite element analyses are also conducted on three-dimensional models for the pin-loaded and clamped SE(T) fracture specimens described previously. The analysis matrix includes the same crack configurations as defined before covering $a/W = 0.1$–0.7 with increments of 0.1, $H/W = 6$ (pin-loaded ends) and $H/W = 10$ (clamped ends) with weld groove width, $2h = 15$ mm. To assess the effects of thickness on the plastic η-factor, the 3-D numerical computations are performed on finite element models for 1-T ($B = 25$ mm) and 0.5-T ($B = 12.5$ mm) fracture specimens with conventional geometry

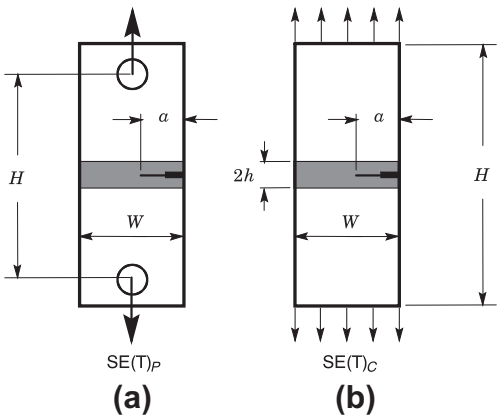

Fig. 2. Geometries for analyzed center notch welded SE(T) fracture specimens with square grooved welds: (a) pin-loaded specimens; (b) clamped specimens.

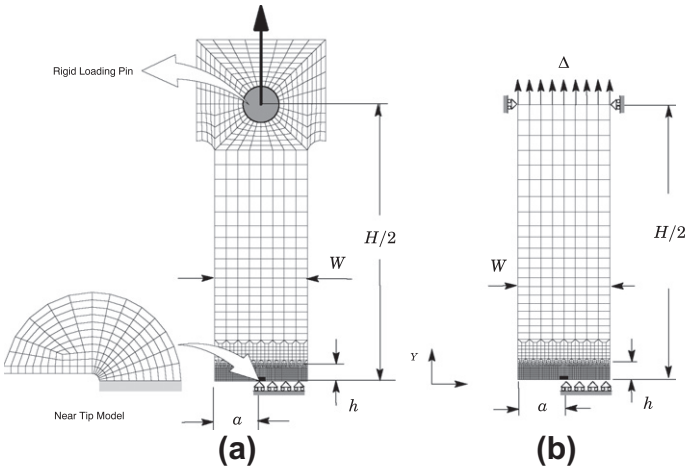

Fig. 3. Finite element models having a square grooved weld with $2h = 15$ mm used in plane-strain analyses; (a) pin-loaded SE(T) specimen with $a/W = 0.5$ and $H/W = 6$; (b) clamped SE(T) specimen with $a/W = 0.5$ and $H/W = 10$.

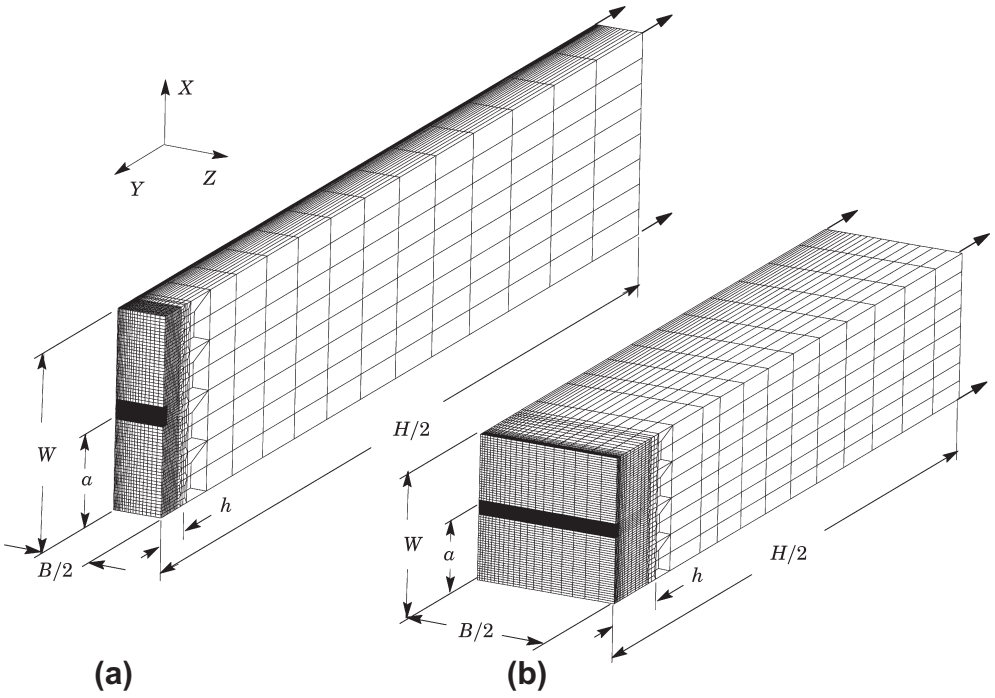

Fig. 4. 3D Finite element models with a square grooved weld of $2h = 15$ mm: (a) pin-loaded SE(T) specimen with $a/W = 0.5$ and $H/W = 6$; (b) clamped SE(T) specimen with $a/W = 0.5$ and $H/W = 10$.

($W/B = 2$). Further finite element analyses also employ a modified geometry with pin load and clamped ends having $B = 30$ mm, $H/W = 10$ and $W/B = 0.5$. This crack configuration, hereafter denoted $B \times B/2$ configuration, is recommended by DNV F-108 procedure [3] for experimental measurements of crack growth resistance curves of pipeline steels and their weldments using fracture specimens extracted from the longitudinal direction of the pipe.

Fig. 4a shows the finite element model constructed for the 3-D analyses of the deeply cracked, 1-T clamped SE(T) specimen ($a/W = 0.5$) with $H/W = 10$ (conventional geometry). Fig. 4b displays the 3-D numerical model of the modified geometry ($W/B = 0.5$) for the deeply cracked, clamped SE(T) specimen ($a/W = 0.5$) with $H/W = 10$. Again, for both geometries, a conventional mesh configuration having a focused ring of elements surrounding the crack front is used with a small key-hole at the crack tip where the radius of the key-hole, ρ_0, is also 2.5 μm (0.0025 mm). Symmetry conditions permit modeling of only one quarter of the specimen with appropriate constraints imposed on the remaining ligament. A typical quarter-symmetric, 3-D

model has 20 variable thickness layers with ~30,000 8-node, 3D elements (~35,000 nodes) defined over the half-thickness ($B/2$); the thickest layer is defined at $Z = 0$ with thinner layers defined near the free surface ($Z = B/2$) to accommodate strong Z variations in the stress distribution. These finite element models are also loaded by displacement increments imposed on the loading points with contact analysis included in the numerical computations of the pin-loaded specimens.

3.3. Material models

Evaluation of factor η requires non-linear finite element solutions which include the effects of plastic work on $J(\delta)$ and the load–displacement response. These analyses utilize an elastic–plastic constitutive model with J_2 flow theory and conventional Mises plasticity in small geometry change (SGC) setting. The numerical solutions employ a simple power-hardening model to characterize the uniaxial true stress-logarithmic strain in the form

$$\frac{\bar{\varepsilon}}{\varepsilon_{ys}} = \frac{\bar{\sigma}}{\sigma_{ys}}, \quad \bar{\varepsilon} \leqslant \varepsilon_{ys}; \quad \frac{\bar{\varepsilon}}{\varepsilon_{ys}} = \left(\frac{\bar{\sigma}}{\sigma_{ys}}\right)^{n}, \quad \bar{\varepsilon} > \varepsilon_{ys} \tag{9}$$

where σ_{ys} and ε_{ys} are the yield stress and strain, and n is the strain hardening exponent. Numerical analyses reveal that use of large geometry change (LGC) setting has essentially no effect on the computed η-factors while weakly affecting the crack-tip loading parameters (J and CTOD). In particular, the scheme adopted here to compute the CTOD (see next section) proves adequate in eliminating the influence of the near-tip blunting region on the (actual) crack tip opening. The SGC solutions facilitate the analyses by eliminating numerical difficulties associated with convergence issues when large geometry changes are included.

The finite element analyses consider material flow properties covering a relatively wide range of strength mismatch: evenmatch and 10%, 20%, 30% and 50% overmatch ($M_y = 1.0$, 1.1, 1.2, 1.3 and 1.5 – see Eq. (7)). The welds are modeled as a bimaterial system (the heat affected zone, HAZ, is not considered in the present work) with the yield stress and hardening property of the base plate adopted as fixed in all analyses and assigned the following properties: $n = 10$ and $\sigma_{ys} = 412$ MPa. Table. 1 provides the material properties utilized in the numerical analyses of the fracture specimens with square groove welds which also consider $E = 206$ GPa and $\nu = 0.3$. The strain hardening parameters for the weld metal are estimated from a simple correlation between the yield stress and hardening exponent applicable for typical structural steels: $n = 5$ and $E/\sigma_{ys} = 800$ (high hardening material), $n = 10$ and $E/\sigma_{ys} = 500$ (moderate hardening material), $n = 20$ and $E/\sigma_{ys} = 300$ (low hardening material). These ranges of properties also reflect the upward trend in yield stress with the increase in strain hardening exponent characteristic of ferritic steels. The hardening exponents for the weld metal are given by linear interpolation of the previous adopted values for σ_{ys} and n.

3.4. Computational procedures

The finite element code WARP3D [21] provides the numerical solutions for the plane-strain analyses reported here. The code enables conventional linear elastic analysis and incorporates a Mises (J_2) constitutive model in both small-strain and finite-strain framework. Evaluation of the J-integral derives from a domain integral procedure [22] which yields J-values retaining strong path independence for domains defined outside the highly strained material near the crack tip. For the 3D analyses reported in Section 4.3, a thickness average value for J is computed over domains defined outside the material having the highly nonproportional histories of the near-tip fields but which is nevertheless well inside the weld metal region.

Evaluation of the numerical value of CTOD follows the 90° procedure [2] to the deformed crack flanks. To avoid potential problems with the CTOD computation related to the severe mesh deformation at the crack tip, the approach adopted here defines the value of half the crack tip opening displacement as the intercept between a straight line at 45° from the crack tip and a straight line passing through selected nodes at the crack flank. The straight line defined by the deformed crack flank nodes is obtained by a linear regression of the corresponding nodal displacements (see details in [14,23]). Numerical analyses reveal that this approach simplifies evaluation of the CTOD while, at the same time, providing very consistent values when the finite elements at the crack tip become highly distorted.

The numerical simulation of the pin loading process involves the contact interaction between the loading pin (represented as a rigid cylinder) and the specimen. WARP3D uses a simple penalty method to enforce displacement constraints

Table 1
Material properties adopted in the analyses of the weldments.

Mismatch level	Weld		Baseplate	
	σ_{ys} (MPa)	n	σ_{ys} (MPa)	n
10% Overmatch	453	11.5	412	10
20% Overmatch	494	12.8	412	10
30% Overmatch	536	14.5	412	10
50% Overmatch	618	17.4	412	10
Evenmatch	412	10	412	10

in the solution of the finite element model which creates springs at the contact points. The spring stiffness corresponds to the penalty parameter, while the amount of remaining penetration corresponds to the error in the enforcement of the constraint. WARP3D adds each spring stiffness into the corresponding element stiffness matrices instead of directly into the global stiffness matrix.

4. Plastic *eta* factors for weld centerline notched SE(T) specimens

The following sections provide the key results for the extensive numerical analyses conducted in pin-loaded and clamped SE(T) with varying crack configuration and different levels of weld strength mismatch. These analyses include plane-strain and 3-D results of the η-factors applicable to determine J and CTOD in weld centerline notched SE(T) specimens derived from experimentally measured load-CMOD records. In the presentation that follows, the plastic η-factors for the analyzed crack configurations are evaluated from solving Eqs. (2) and (6) upon computation of the plastic area, A_p under the load–displacement (CMOD or LLD) curve. The scheme to determine the dimensionless factor η_J (the process to evaluate factor η_δ is analogous) was already provided in Part I of this article [14]. Here, we note that these η-factors are determined based upon a least square fit to the computed evolution of J with plastic area, A_p, in the range 100–1000 kJ/m^2 and its corresponding range of CTOD values. This procedure maintains consistency with typical toughness levels for common structural steels measured using SE(T) specimens (refer to Part I of this investigation [14]). Numerical analyses reveal that small changes in the range of J (CTOD) values over which the least square fitting is performed does not essentially affect the computed η-values. The research code FRACTUS2D [23] is employed throughout all the computations reported here.

4.1. Plane-strain η-factors

The extensive plane-strain analyses performed on models of the pin-loaded and clamped SE(T) specimens with centerline-cracked welds described previously cover nondimensional η-factors based upon P-LLD and P-CMOD records for crack configurations with $H/W = 6$ (pin-loaded ends) and $H/W = 10$ (clamped ends) with weld groove size, $2h = 15$ mm, including varying weld groove sizes ($h/W = 0.1$, 0.15, 0.20 and 0.40 – refer to Section 3.1) and different levels of weld strength mismatch ($M_y = 1.0$, 1.1, 1.2, 1.3 and 1.5 – see Eq. (7)). Here, the analyses for the weld centerline notched configurations with $2h = 15$ mm provide the baseline values upon which J and CTOD estimation equations for welded SE(T) fracture specimens are later derived.

Figs. 5–7 provide factors η_J derived from CMOD (η_J^{CMOD}) and LLD (η_J^{LLD}) and factors η_δ based on CMOD ($\eta_\delta^{\mathrm{CMOD}}$) for the pin-loaded and clamped SE(T) specimens with varying a/W-ratios and different mismatch levels for the groove size $2h = 15$ mm. In these plots, the solid symbols correspond to the computed η-values whereas the lines represent fitting curves to the numerical data. For comparison, Figs. 5 and 7 also include the plastic η-solutions for homogeneous pin-loaded specimens derived from previous work of Kim and Budden [13]. Based on the previous findings discussed in Part I of this article [14] in which accurate evaluation of J (and, equivalently, CTOD) based on the η-method for very shallow cracked specimens was questioned, these fitting curves are provided only in the range $0.2 \leqslant a/W \leqslant 0.7$ (the description of the fitting procedure is postponed until the end of this section). Section 5 also addresses this issue and show results for the weld centerline notched specimens based upon the multispecimen methodology.

Consider first the variation of η_J^{CMOD} with increased a/W-ratio and different mismatch levels shown in Figs. 5a and 6a. Here, factor η_J derived from CMOD is less sensitive to the degree of mismatch for shallow cracked specimens ($0.2 \leqslant a/W \leqslant 0.3$) whereas the dependence of η_J^{CMOD} on M_y is slightly more pronounced for deeply cracked specimens ($0.4 \leqslant a/W$). Similar trends are also exhibited by the variation of η_J^{LLD} with increased a/W-ratio and different mismatch levels shown in Fig. 7. Consider now the variation of plastic η-factors to determine the plastic component of CTOD, defined by $\eta_\delta^{\mathrm{CMOD}}$, with increased a/W-ratio and different mismatch levels shown in Figs. 5b and 6b. Compared to the previous results, the effect of M_y on η_δ is similar but relatively uniform irrespective of a/W-ratio.

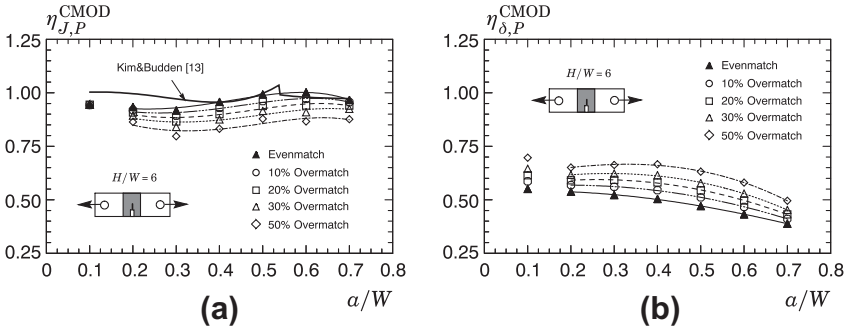

Fig. 5. Variation of plastic factors η_J and η_δ with a/W-ratio derived from CMOD for plane-strain analyses of pin-loaded SE(T) specimens with varying strength mismatch levels.

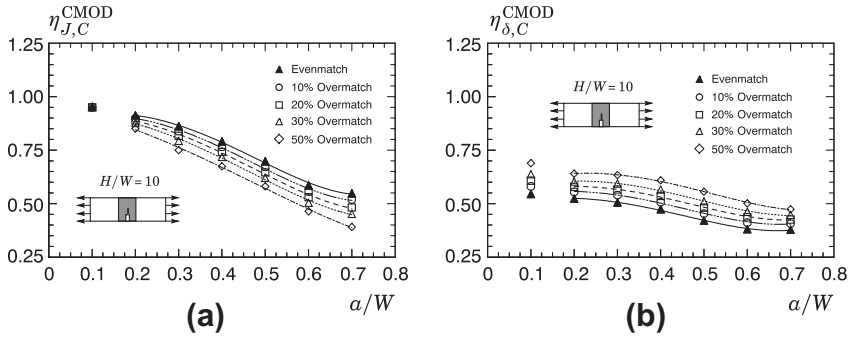

Fig. 6. Variation of plastic factors η_J and η_δ with a/W-ratio derived from CMOD for plane-strain analyses of clamped SE(T) specimens with varying strength mismatch levels.

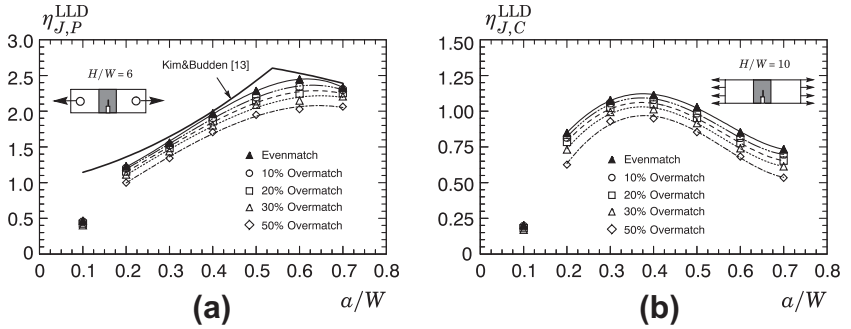

Fig. 7. Variation of plastic factor η_J with a/W-ratio derived from LLD for plane-strain analyses of pin-loaded and clamped SE(T) specimens and varying strength mismatch levels.

The results displayed in these plots reveal general trends in that factors η_J and η_δ are relatively insensitive to the degree of strength mismatch, particularly for mismatch levels in the range of 10–20% overmatch ($My \leqslant 1.2$) for shallower cracked specimens ($0.2 \leqslant a/W \leqslant 0.3$). However, higher mismatch levels (30% and 50% overmatch) cause a slightly more prominent departure from the evenmatch condition in which the corresponding η_J and η_δ-values differ by 20–30%. The behavior exhibited by these plots contrasts rather sharply with the general effects of strength mismatch on plastic η-factors for bend crack configurations as revealed in previous work of Donato et al. [26]. In their analyses, factors η_J and η_δ display more sensitivity on the degree of strength mismatch, particularly for shallow crack geometries.

Now, to provide a simpler manipulation of the previous results and using the plots displayed in Figs. 5–7 for guidance, a functional dependence of factors η_J and η_δ with crack size and strength mismatch level is constructed in the form

$$\eta(a/W) = C_0 + C_1(a/W) + C_2(a/W)^2 + C_3(a/W)^3 \tag{10}$$

where it is understood that a 3-rd order polynomial fitting is employed and coefficients C_k are function of the mismatch level, i.e., $C_k = f(M_y)$ which are also described by a 3-rd order polynomial fitting as

$$C_k = \xi_0 + \xi_1 M_y + \xi_2 M_y^2 + \xi_3 M_y^3 \tag{11}$$

A standard least square fitting to the computed values displayed in the plots of Figs. 5–7 then provides the coefficients C_k and ξ_k as given in Tables. 2–4. Here, for a given coefficient C_k needed to determine factor $\eta(a/W)$ by means of Eq. (10), the corresponding line in Tables. 2–4 (which depends on specimen configuration and whether η_J or η_δ is required) then provides coefficients ξ_k for use in Eq. (11). Again, we note that these fitting curves are essentially valid in the range $0.2 \leqslant a/W \leqslant 0.7$ and $1.0 < M_y \leqslant 1.5$. Moreover, previous work by Cravero and Ruggieri [4] have demonstrated that the η-factors for pin-loaded SE(T) specimens are not affected by the pin loading distance or the H/W-ratio; consequently, these numerical results are understood to represent all applicable values of η-factors for this crack configuration having a wide range of pin loading distance relative to specimen width.

4.2. Effects of weld groove size on plastic η-factors

To examine the effects of weld groove size on the plastic η-factors, consider now the analyses of weld centerline notched SE(T) specimens with varying groove width. Figs. 8–11 provide the dependence of η_J and η_δ on the degree of strength

Table 2
Coefficients for the polynomial fitting of factor η_J given by Eqs. (10) and (11) for CMOD data.

Specimen	H/W	C_k	ξ_0	ξ_1	ξ_2	ξ_3
SE(T)$_P$	All	C_0	1.9221	−1.4804	0.8804	−0.1267
		C_1	−7.4583	9.2930	−4.1260	−0.1597
		C_2	20.2120	−17.5470	−0.3149	4.3608
		C_3	−16.8740	11.6610	5.3814	−5.4275
SE(T)$_C$	10	C_0	3.5804	−7.3516	6.0628	−1.5442
		C_1	−16.8870	49.8030	−41.2640	10.2260
		C_2	35.8190	−108.5900	87.4780	−20.9510
		C_3	−26.3000	78.2410	−61.9790	14.5380

Note: Polynomial fitting valid in the range $0.2 \leqslant a/W \leqslant 0.7$ and $1.0 < M_y \leqslant 1.5$.

Table 3
Coefficients for the polynomial fitting of factor η_J given by Eqs. (10) and (11) for LLD data.

Specimen	H/W	C_k	ξ_0	ξ_1	ξ_2	ξ_3
SE(T)$_P$	All	C_0	5.6260	−5.5766	0.6577	0.4201
		C_1	−62.4380	98.4230	−43.5050	4.9874
		C_2	226.5500	−372.4200	197.9700	−33.3190
		C_3	−208.4500	354.7100	−201.8200	37.4130
SE(T)$_C$	10	C_0	−1.0542	1.7027	−1.3109	0.1157
		C_1	1.4650	19.6500	−15.1360	4.7893
		C_2	23.5690	−98.1900	72.4170	−19.3620
		C_3	−32.5610	99.6160	−73.2560	18.7580

Note: Polynomial fitting valid in the range $0.2 \leqslant a/W \leqslant 0.7$ and $1.0 < M_y \leqslant 1.5$.

Table 4
Coefficients for the polynomial fitting of factor η_δ given by Eqs. (10) and (11) for CMOD data.

Specimen	H/W	C_k	ξ_0	ξ_1	ξ_2	ξ_3
SE(T)$_P$	All	C_0	1.1081	−1.1825	0.7314	−0.1211
		C_1	−8.7010	16.4220	−9.1314	1.5208
		C_2	19.9310	−42.3550	27.3720	−5.4822
		C_3	−14.1030	32.6610	−23.8610	5.4091
SE(T)$_C$	10	C_0	−0.7970	2.7661	−2.1985	0.6108
		C_1	2.8337	−6.4921	7.7836	−2.6687
		C_2	0.8604	−6.4540	−0.5223	1.6885
		C_3	−5.7972	18.3860	−10.9500	1.7016

Note: Polynomial fitting valid in the range $0.2 \leqslant a/W \leqslant 0.7$ and $1.0 < M_y \leqslant 1.5$.

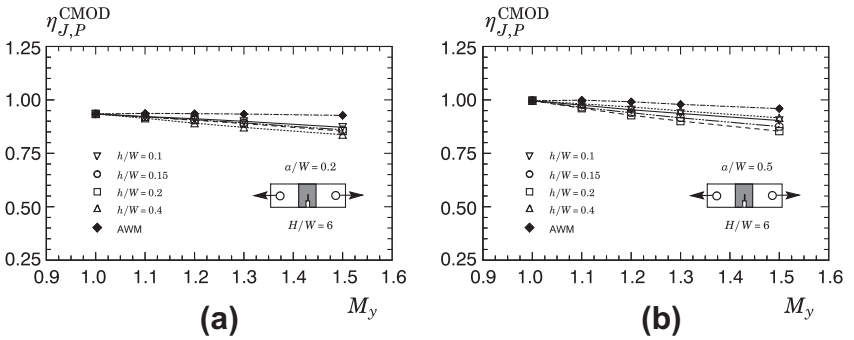

Fig. 8. Dependence of plastic factor η_J derived from CMOD on weld groove size (h/W-ratio) for plane-strain analyses of pin-loaded SE(T) specimens and varying strength mismatch levels.

mismatch with different h/W-values for shallow ($a/W = 0.2$) and deep ($a/W = 0.5$) crack configurations under pin load and clamp conditions. These plots also include η-factors corresponding to the condition referred to as "all weld metal" (AWM) in which the fracture specimens are made of a homogeneous material having the weld metal properties

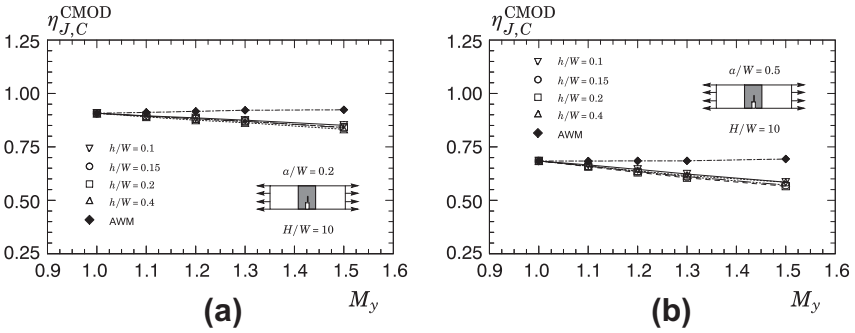

Fig. 9. Dependence of plastic factor η_J derived from CMOD on weld groove size (h/W-ratio) for plane-strain analyses of clamped SE(T) specimens and varying strength mismatch levels.

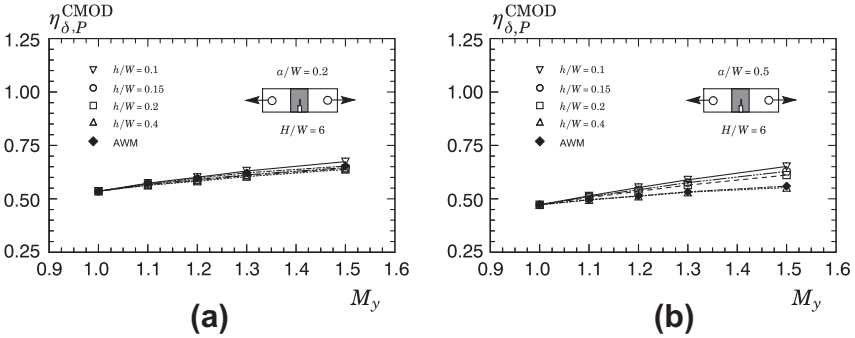

Fig. 10. Dependence of plastic factor η_δ derived from CMOD on weld groove size (h/W-ratio) for plane-strain analyses of pin-loaded SE(T) specimens and varying strength mismatch levels.

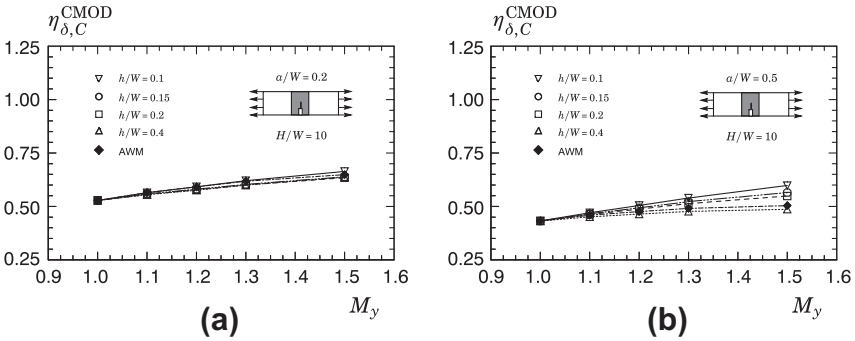

Fig. 11. Dependence of plastic factor η_δ derived from CMOD on weld groove size (h/W-ratio) for plane-strain analyses of clamped SE(T) specimens and varying strength mismatch levels.

corresponding to the mismatch condition (refer to Table. 1 previously described). These results clearly reveal a weak dependence of factors η_J on weld groove size for the entire range of mismatch level for all analyzed crack configurations. The sensitivity of η_δ on h/W also follows very similar trends, particularly for the shallow crack configuration under pin load and clamp conditions. In contrast, the results for the deeply cracked specimens display a slightly different behavior in which factor η_δ for the 50% overmatch condition (M_y = 1.5) shows a more pronounced variation with h/W; however, the weak effect of weld groove size on η_δ persists for $M_y \leqslant 1.3$. The dependence of factors η_J^{CMOD} on M_y for the all weld metal condition also deserves attention. Here, we note that the η_J^{CMOD}-factors for both the pin-load and clamped specimen are essentially constant irrespective of the weld metal properties. Such behavior simply reflects the weak dependence of factor η_J^{CMOD} on the material's flow properties as already described in Part I of this article [14]. Overall, these results provide a strong support to use the plastic η-factors presented previously in Figs. 5–7 as representative values used in J and CTOD estimation procedures for weld centerline notched SE(T) fracture specimens irrespective of weld groove size in the range h/W = 0.1–0.40.

4.3. Three-dimensional effects on plastic η-factors

The plastic η-factors for pin-loaded and clamped SE(T) specimens provided in previous section are based upon detailed plane-strain analyses for these crack configurations with varying crack sizes and different levels of weld strength mismatch. However, the 3D character of the crack-tip strain–stress fields coupled with potential mismatch effects between the base plate and weld metal may affect the plastic contribution to the strain energy of the cracked body upon which factor η is determined. To examine the effects of out-of-plane constraint associated with specimen thickness on the η-factors, additional analyses on 3-D models for pin-loaded and clamped SE(T) configurations with 20% overmatch ($M_y = 1.2$) and 50% overmatch ($M_y = 1.5$) having weld groove size $2h = 15$ mm are conducted. These 3-D finite element models were described previously and include pin-loaded ($H/W = 6$) and clamped specimens ($H/W = 10$) having standard geometry ($B \times 2B$) with $B = 25$ mm (1-T) and 12.7 mm (0.5-T). The analyses also consider 3-D models for pin-loaded and clamped specimens with a modified geometry having $B \times B/2$ with $B = 30$ mm; this specimen configuration is adopted by DNVF-108 [3] in experimental measurements of crack growth resistance curves of pipeline steels and their weldments using fracture specimens extracted from the longitudinal direction of the pipe.

Figs. 12–15 compare the plastic factors η_J and η_δ derived from CMOD for these crack configurations based upon the 3-D analyses with varying crack sizes (a/W). To facilitate comparison of the results, the plots also include the plane-strain η-values described previously. Apart from small differences (which depend upon crack size and specimen configuration), the computed three-dimensional η-values are essentially similar to the corresponding plane-strain values for the 20% overmatch condition ($M_y = 1.2$). However, a rather different picture emerges for the 50% overmatch condition ($M_y = 1.5$). While factors η_J and η_δ derived from CMOD for the standard geometry, $B \times 2B$ with $B = 25$ mm (1-T) and 12.7 mm (0.5-T), are essentially similar to the corresponding plane-strain values, the η-values for the specimen configuration with $B \times B/2$ (as recommended by DNV F-108 [3]) exhibit differences in the range 20–25%; here, η_J-values are higher whereas η_δ-values are lower with respect to the baseline plane-strain η-values. Such differences arise from the coupled effect of weld grove size (which has a fixed value of $2h = 15$ mm in these analyses) relative to the remaining crack ligament, $b = (W-a)$, and degree of weld strength mismatch. Consider the standard geometry with $B = 12.5$ mm (0.5-T), $W = 25$ mm and $a/W = 0.5$ in which $b = 12.5$ mm; here, the b/h-ratio is $\sim$1.7. Consider now the specimen configuration with $B \times B/2$ with $B = 30$ mm, $W = 15$ mm and $a/W = 0.5$ in which $b = 7.5$ mm thereby resulting in $b/h = 1$. For a fixed loading level (as measured by J) and degree of weld strength mismatch for both crack configurations, the relationship between J and plastic area under the P-CMOD curve (upon which η is derived) is altered. Indeed, Eripret and Hornet [27] and Hornet et al. [28] discuss this issue and point out that the global behavior of mismatched fracture specimens may be strongly affected by the level of strength mismatch coupled with the relative weld groove size.

The above results and discussions can therefore be summarized as follows: (1) the plane-strain values describe well the variation of η-values with a/W for moderate degrees of mismatch ($M_y \leqslant 1.2$); (2) the η-factors are only slightly affected by 3-D effects associated with specimen thickness (out-of-plane constraint); here, the η-values for the $B \times B/2$ configuration are somewhat more sensitive to specimen size but which are nevertheless in close correspondence to the 0.5-T and 1-T geometries; (3) the plane-strain values provide conservative η_J-factors when compared to corresponding 3-D results for the specimen configuration with $B \times B/2$ (which is adopted by DNV F-108 [3]) in case of higher degrees of overmatch ($M_y = 1.5$). Such observation appears particularly important when determining the CTOD from the J-integral as currently adopted by a number of procedures (see, e.g., ASTM 1290 [24] and DNV F-101 [25]).

5. Relationship between J and plastic work in weld centerline notched SE(T) specimens

In Part I of this article [14], the mechanical energy balance between the work done by external forces and the strain energy due to the crack was advantageously analyzed to explore the quantitative effects of any plasticity development well

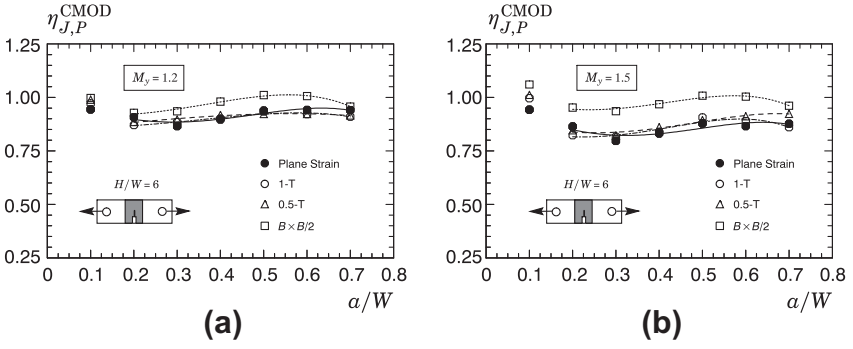

Fig. 12. Comparison of plastic factors η_J derived from CMOD for pin-loaded SE(T) specimens with different strength mismatched welds based on plane-strain and 3-D analyses.

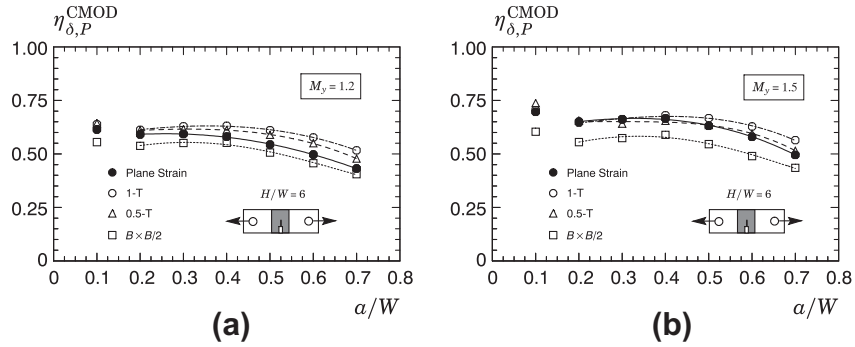

Fig. 13. Comparison of plastic factors η_δ derived from CMOD for pin-loaded SE(T) specimens with different strength mismatched welds based on plane-strain and 3-D analyses.

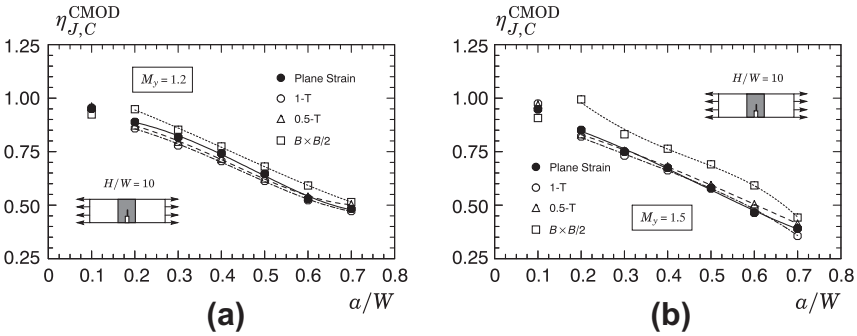

Fig. 14. Comparison of plastic factors η_J derived from CMOD for clamped SE(T) specimens with different strength mismatched welds based on plane-strain and 3-D analyses.

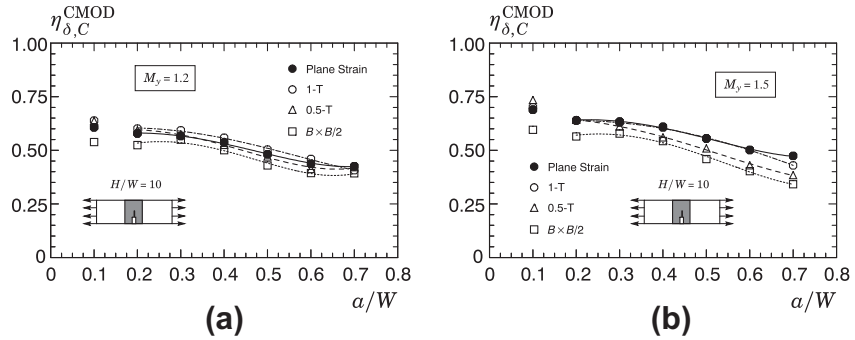

Fig. 15. Comparison of plastic factors η_δ derived from CMOD for clamped SE(T) specimens with different strength mismatched welds based on plane-strain and 3-D analyses.

outside the crack-tip region on J for a homogeneous specimen. It was shown that the total plastic work does not translate into equivalent values of J for very shallow cracked specimens ($a/W < 0.2$). In what follows now, we consider application of the multispecimen procedure outlined previously in Section 2.2 to evaluate the J-integral for weld centerline notched SE(T) fracture specimens with varying levels of weld strength overmatch and different crack sizes. The study pursued here is directed toward answering the following question: under what conditions the potential energy change for a cracked body (based upon which J is defined) is equivalent to the plastic work for the stressed cracked body described in terms of the area under the load–displacement curve (based upon which factor η is defined)? The energy release rate definition of J given in previous Section 2.2 represents a mechanical energy balance between the work done by external forces and the strain energy due to the crack. It becomes clear that any plasticity development well outside the crack-tip region provides an additional

contribution to the strain energy for the cracked component which therefore affects the plastic area under the load–displacement curve. Under such conditions, the total plastic work does not necessarily translate into a corresponding value of J for the cracked body.

Fig. 16 displays the variation of J with load-line displacement (LLD or Δ) for selected specimen configurations which include pin load ($H/W = 6$) and clamped end ($H/W = 10$) conditions with a very shallow ($a/W = 0.1$) and a deep ($a/W = 0.5$) crack for the 20% overmatch weld. The behavior exhibited by these J-Δ trajectories is consistent with previous findings reported in Part I [14]. For the deeply cracked geometries ($a/W = 0.5$), the J-values computed using the line-integral definition, J_D, on a remote contour ahead of crack tip are essentially the same as the corresponding values derived from Eq. (8). In contrast, the J-values derived from the multispecimen procedure, J_M, differ significantly from the corresponding line-integral definition of J for the very shallow crack specimen ($a/W = 0.1$). Very similar trends were observed for additional analyses using other overmatch conditions; these results are not shown here to conserve space.

Because a rigorous equivalence between plastic work and the strain energy for the cracked body upon which J is defined does not hold true when CMOD measurements are employed [6], the previous limitation on the use of η_J^{LLD}-values in very shallow notch specimens ($a/W < 0.2$) may not necessarily apply when η_J^{CMOD}-values are used. However, a number of studies show a close correspondence between factors η_J^{LLD} and η_J^{CMOD} (refer, for example, to the work Kim and Budden [13] and Cravero and Ruggieri [6]), even though experimental observations reveal that CMOD measurements are less sensitive to remote deformation than LLD data. Work along this line of investigation is in progress and the present analyses proceed with the assumption that η_J^{LLD} relates to η_J^{CMOD} as already discussed in Part I [14].

Fig. 17 compares the J-values derived from the multispecimen procedure, J_M, against the corresponding J-values computed using the line-integral definition, J_D, for the pin loaded ($H/W = 6$) and clamped ($H/W = 10$) specimens with varying crack sizes ($a/W = 0.1$, 0.2 and 0.5) and different degrees of weld overmatch (20% and 50% overmatch). Each curve provides pairs of J-values, J_M vs. J_D, for the weld centerline notched SE(T) specimen computed at the same LLD-value. Reference lines are shown which define a constant J-ratio, e.g., $J_M = 1.2 \times J_D$ which implies a 20% difference between J_M and J_D. The results shown in these plots for each crack configuration (pin load vs. clamp conditions) display only little sensitivity on the level of weld overmatch. However, a strong crack size dependence of the J_M vs. J_D curves can be seen, notably in the shallow crack range. The J-values computed using the line-integral definition differ by 20% or less of the corresponding values derived from Eq. (8) for the crack configurations with $a/W > 0.2$, particularly the clamped SE(T) fracture specimens. In contrast, the J_M vs. J_D curve for the very shallow crack configuration deviate dramatically from the reference lines. It may be recalled that such behavior follows precisely similar results already presented in Part I for homogeneous SE(T) specimens with the added observation of the relative minor role played by the degree of weld overmatch. Consistent with the previous study, these features provide additional concern on the application of SE(T) fracture specimens with very shallow cracks ($a/W < 0.2$) in current testing protocols for toughness measurements and defect assessment applications.

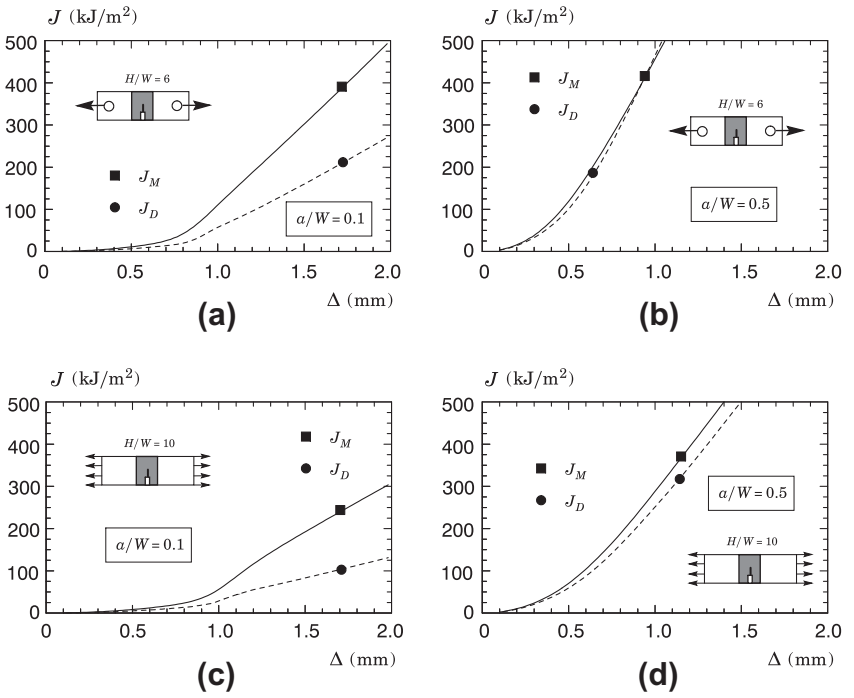

Fig. 16. Evolution of J with load-line displacement (Δ) for pin-loaded and clamped SE(T) specimen with 20% overmatch weld and selected a/W-ratios.

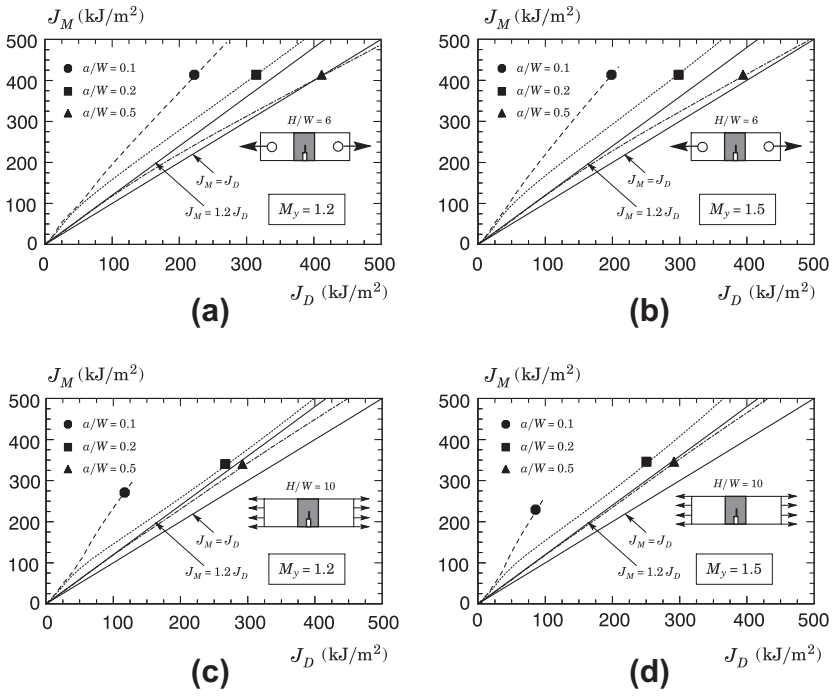

Fig. 17. Evolution of J_M with J_D for pin-loaded and clamped SE(T) specimen with 20% and 50% overmatch weld and selected a/W-ratios.

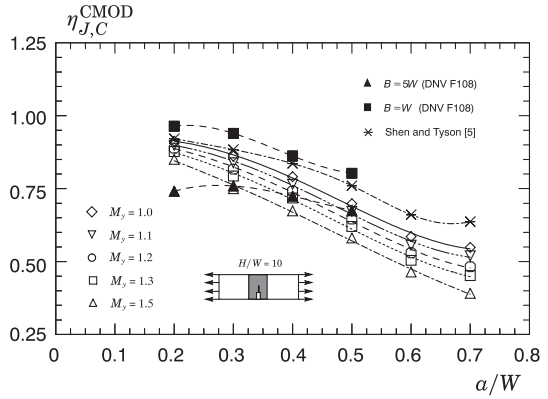

Fig. 18. Comparison of present plane-strain η_J-values derived from CMOD with previously published results.

6. Concluding remarks

This work addresses the effect of weld strength mismatch on J and CTOD estimation formulas which are mainly applicable to determine fracture toughness parameters from laboratory measurements of load–displacement data using clamped SENT fracture specimens with a square groove, center crack weld. The plane-strain results reveal that levels of weld strength mismatch within the range of 10–20% mismatch do not affect significantly J and CTOD estimation expressions applicable to homogeneous materials, particularly for shallow cracked fracture specimens. Another central result emerging from the analyses conducted here is that the plastic η-factors depend weakly on specimen thickness since 3-D effects on the η-values are very small. Moreover, the present analyses reveal that the plane strain η-values are generally smaller (albeit differences are not significant) than the corresponding 3-D results. Such important observations suggest that plane-strain values should be used in estimation procedures of J and CTOD from experimentally measured load–displacement records to obtain rather conservative toughness measures. The fitting equations describing factors η_J^{LLD}, η_J^{CMOD} and $\eta_\delta^{\mathrm{CMOD}}$ provided here serve to this purpose. Comparisons of the plane-strain η_J^{CMOD}-values for the clamped SENT specimens having $H/W = 10$ with previously reported η-factors [3,5] further demonstrate the applicability of the estimation procedure for J (and CTOD) developed here. Fig. 18 recasts factors η_J^{CMOD} displayed in previous Fig. 6a and includes η-values based on CMOD from DNV F-108 [3] and the

numerical analyses conducted by Shen and Tyson [5]. The DNV equation describing the η-factors for clamped SENT specimens is valid for $0.2 \leqslant a/W \leqslant 0.5$ and also incorporates a thickness correction applicable in the range $1 \leqslant B/W \leqslant 5$. This plot shows clearly different trends on the variation of η_J^{CMOD} with increasing a/W-ratio and varying mismatch levels.

Acknowledgments

This investigation is supported by Fundação de Amparo à Pesquisa do Estado de São Paulo (FAPESP) through a graduate scholarship (2008/54208-3) provided to the first author (MP). The work of CR is supported by the Brazilian Council for Scientific and Technological Development (CNPq) through Grants 304132/2009-8 and 476581/2009-5 and also by FAPESP through Grant 09/54229-3.

References

[1] Hutchinson JW. Fundamentals of the phenomenological theory of nonlinear fracture mechanics. J Appl Mech 1983;50:1042–51.
[2] Anderson TL. Fracture mechanics: fundaments and applications. 3rd ed. Boca Raton: CRC Press; 2005.
[3] Det Norsk Veritas. Fracture control for pipeline installation methods introducing cyclic plastic strain. Recommended practice DNV-RP-F108; 2006.
[4] Cravero S, Ruggieri C. Estimation procedure of *J*-resistance curves for SE(T) fracture specimens using unloading compliance. Engng Fract Mech 2007;74:2735–57.
[5] Shen G, Tyson WR. Crack size evaluation using unloading compliance in Single – specimen single-edge-notched tension fracture toughness testing. J Test Eval 2009;37(4) [paper ID JTE102368].
[6] Cravero S, Ruggieri C. Further developments in *J* evaluation procedure for growing cracks based on LLD and CMOD data. Int J Fract 2008;148:387–400.
[7] Nyhus B, Polanco M, Ørjasæter O. SENT Specimens as an alternative to SENB specimens for fracture mechanics testing of pipelines. In: ASME international conference on offshore mechanics and arctic engineering (OMAE 2003). Cancun (Mexico): American Society of Mechanical Engineers; 2003.
[8] Cravero S, Ruggieri C. Correlation of fracture behavior in high pressure pipelines with axial flaws using constraint designed test specimens – part I: plane-strain analyses. Engng Fract Mech 2005;72:1344–60.
[9] Silva LAL, Cravero S, Ruggieri C. Correlation of fracture behavior in high pressure pipelines with axial flaws using constraint designed test specimens – part II: 3-D effects on constraint. Engng Fract Mech 2006;73:2123–38.
[10] Donato GHB, Ruggieri C. Constraint effects and crack driving forces in surface cracked pipes subjected to reeling. In: ASME international conference on offshore mechanics and arctic engineering (OMAE 2008). Lisbon (Portugal): American Society of Mechanical Engineers; 2008.
[11] Shen G, Bouchard R, Gianetto JA, Tyson WR. Fracture toughness evaluation of high-strength steel pipe. In: ASME PVP 2008 pressure vessel and piping division conference (PVP 2008). Chicago (IL): American Society of Mechanical Engineers; 2008.
[12] Park DY, Tyson WR, Gianetto JA, Shen G, Eagleson RS. Evaluation of fracture toughness of X100 pipe steel using SE(B) and clamped SE(T) single specimens. In: ASME international pipeline conference (IPC 2010). Calgary (Canada): American Society of Mechanical Engineers; 2010.
[13] Kim YJ, Budden PJ. Plastic η factor solutions of homogeneous and Bi-material SE(T) specimens for toughness and creep crack growth testing. Fatigue Fract Engng Mater Struct 2001;24:751–60.
[14] Ruggieri C. Further results in J and CTOD estimation procedures for SE(T) fracture specimens – part I: homogeneous materials. Eng Fract Mech 2012;79:245–65.
[15] Sumpter JDG, Turner CE. Method for laboratory determination of Jc, cracks and fracture, ASTM STP 601, American Society for Testing and Materials; 1976. p. 3–18.
[16] Kanninen MF, Popelar CH. Advanced fracture mechanics. New york: Oxford University Press; 1985.
[17] Kirk MT, Dodds RH. *J* and CTOD estimation equations for shallow cracks in single edge notch bend specimens. J Test Eval 1993;21:228–38.
[18] Shih CF. Relationship between the *J*-integral and the crack opening displacement for stationary and extending cracks. J Mech Phys Solids 1981;29:305–26.
[19] British Standard. Fracture mechanics toughness tests, BS 7448; 1991.
[20] Begley JA, Landes JD. The J integral as a fracture criterion, fracture toughness, ASTM STP 514. Philadelphia: American Society for Testing and Materials; 1972. p. 1–20.
[21] Gullerud A, Koppenhoefer K, Roy A, RoyChowdhury S, Walters M, Bichon B, et al. WARP3D: dynamic nonlinear fracture analysis of solids using a parallel computers and workstations. Structural research series (SRS) 607. UILU-ENG-95-2012. University of Illinois at Urbana-Champaign; 2004.
[22] Moran B, Shih CF. A general treatment of crack tip contour integrals. Int J Fract 1987;35:295–310.
[23] Ruggieri C. FRACTUS2D: numerical computation of fracture mechanics parameters for 2-D cracked solids EPUSP. University of São Paulo; 2010.
[24] American Society for Testing and Materials. Standard test method for crack-tip opening displacement (CTOD) fracture toughness measurement, ASTM E1290; 2008.
[25] Det Norsk Veritas. Submarine Pipeline Systems. DNV-OS-F101; 2007.
[26] Donato GHB, Magnabosco R, Ruggieri C. Effects of weld strength mismatch on *J* and CTOD estimation procedure for SE(B) specimens. Int J Fract 2009;159:1–20.
[27] Eripret C, Hornet P. Fracture toughness testing procedures for strength mis-matched structures. In: Schwalbe KH, Koçak M, editors. Mis-matching of interfaces and welds. Geesthacht (Germany): GKSS Publications; 1997.
[28] Hornet P, Eripret C, Hao S. Experimental *J* estimation from a load-CMOD curve for mis-matched SENB and CCT specimens. In: Schwalbe KH, Koçak M, editors. Mis-matching of interfaces and welds. Geestchacht (Germany): GKSS Publications; 1997.